Appl. Phys. A 85, 247–253 (2006)
DOI: 10.1007/s00339-006-3708-8

**Applied Physics A**
**Materials Science & Processing**

A. COLLI[1]
S. HOFMANN[1]
A. FASOLI[1]
A.C. FERRARI[1]
C. DUCATI[2]
R.E. DUNIN-BORKOWSKI[2]
J. ROBERTSON[1,✉]

# Synthesis and optical properties of silicon nanowires grown by different methods

[1] Department of Engineering, University of Cambridge, Cambridge CB3 0FA, UK
[2] Department of Materials Science and Metallurgy, University of Cambridge, Cambridge CB3 6GF, UK

**Received: 11 May 2006/Accepted: 3 July 2006**
**Published online: 20 September 2006 •** 

**ABSTRACT** We review our recent results on the growth and characterization of silicon nanowires (SiNWs). Vapour-phase deposition techniques are considered, including chemical vapour deposition (CVD), plasma-enhanced chemical vapour deposition (PECVD), high-temperature annealing, and thermal evaporation. We present complementary approaches to SiNW production. We investigate the low-temperature (down to 300 °C) selective nucleation of SiNWs by Au-catalysed CVD and PECVD. Bulk production of SiNWs is obtained by thermal-vapour deposition from Si/SiO powders in a high-temperature furnace. In this case, SiNWs grow either by condensing on Au catalyst films, or by self-condensation of the vapour in a lower-temperature region of the furnace. Finally, we also achieve controlled growth by thermolysis of nanopatterned, multi-layered Si/Au thin-film precursors. The as-produced wires are compared in terms of yield, structural quality, and optical properties. Raman and photoluminescence spectra of SiNWs are discussed.

**PACS** 81.15.Gh; 73.21.-b; 73.21.Hb; 71.20.Mq; 78.30.-j

## 1 Introduction

Crystalline semiconducting nanostructures have become very popular in recent years both for fundamental physics and their potential applications in electronic and optoelectronic devices [1, 2]. One-dimensional (1D) silicon nanowires (SiNWs) are particularly attractive, due to the central role of silicon in the semiconductor industry. SiNWs have the potential to be used as the active channels into future high-integration electronic devices. SiNW field-effect transistors have been assembled both in planar and vertical geometries [3, 4], and they may exhibit promising transport characteristics compared to planar devices fabricated by top-down approaches [3, 5].

So far, different methods have been used to grow SiNWs, but a universal growth technique fulfilling all the requirements for potential applications has not yet emerged. Chemical vapour deposition (CVD) and plasma-enhanced (PE)CVD have been widely used to produce substrate-bound arrays of SiNWs [6–11]. In this method, patterned Au seeds are used to define the nucleation sites, while oriented crystalline Si surfaces can provide epitaxial nucleation and therefore NW alignment [9]. Controlled doping during synthesis may be achieved by mixing $PH_3$ [10] or $B_2H_6$ [11] into the Si precursor gas. On the other hand, a high yield of free-standing SiNWs has been obtained in a vapour-transport reactor by laser ablation [12, 13] or by simple thermal evaporation of Si solid precursors [14–16]. In most cases, these approaches still require the presence of a metal catalyst to promote the nucleation of one-dimensional structures. With process temperatures usually exceeding 1000 °C, metals (such as Au, Fe, Ga, or Sn) are added to the Si target (when laser ablation is used) or to the Si solid precursor (for thermal evaporation) [12–16]. As a result, nanowires are collected as a wool-like, substrate-free deposit. It has been shown, however, that metal-free SiNWs can also be grown by vapour transport [17, 18]. Since in this case non-stoichiometric SiO is the Si source, it was argued that the oxygen triggers the 1D nucleation process, and therefore this mechanism has been referred to as oxide-assisted growth (OAG). To date, the OAG method provided the highest yield per single growth run, with a bulk production of SiNWs on a mg scale [17].

As most groups focus on a single growth method, it is difficult to derive from the literature a representative figure of merit to compare the different synthesis processes. We have therefore investigated several complementary approaches to SiNW production within the same experimental environment. Here we review our recent results on the growth and characterization of SiNWs. CVD and PECVD allow the selective nucleation of SiNWs down to low temperature, i.e. 300 °C [7]. Bulk production of SiNWs is obtained by thermal vapour deposition from Si/SiO powders in a high-temperature furnace (> 1000 °C). In this case, SiNWs grow either by condensing on Au catalyst films, or by self-condensation of the vapour in a lower-temperature region of the furnace. We also achieve controlled growth by thermolysis of nanopatterned, multi-layered Si/Au thin-film precursors. The as-produced wires are compared in terms of yield, structural quality (diameter, length, curliness, etc.), and optical properties.

✉ E-mail: jr214@hermes.cam.ac.uk

## 2 Experimental

Both catalytic and catalyst-free growth of SiNWs were investigated. Metal-free NWs produced by the oxide-assisted method do not require a substrate, but condense into free-standing bundles. For catalyst-assisted growth, oxidized Si substrates were coated and patterned with thin Au layers (0.5 nm) [7]. Au was deposited by evaporating Au metal from a ceramic boat in a standard evaporator at a base pressure below $10^{-6}$ mbar. The thickness of the Au layer was determined by an in situ quartz crystal.

We studied the low-temperature, catalytic (PE)CVD growth in an Oxford Instruments $\mu$P reactor, capable of a base pressure of $1 \times 10^{-6}$ mbar. The Au-coated Si wafers were heated to 300–380 °C, as monitored by a thermocouple in direct contact with the substrate surface. Then, pure $SiH_4$ was admitted as the Si source gas, the total pressure varying between 200 mTorr and 10 Torr. A 13.6-MHz rf power (10–15 W) was used to create a plasma, except when a thermal reaction was desired.

High-temperature, catalytic growth of SiNWs was studied by means of a simple thermal evaporation process in a horizontal-tube furnace reactor. Pure Si powders (Alpha Aesar, 99.99%) were placed in an alumina boat and heated to 1150–1250 °C. The Si vapour was carried downstream by a 100-sccm Ar flow and condensed along the colder regions of the furnace tube where the Au-coated substrates were placed. Typical substrate temperatures fell in the 750–850 °C range. The Ar pressure was set to 100 mbar during growth and 1 bar during the temperature ramps, to provide pressure-based growth interruptions and avoid non-steady-state effects [19]. An equivalent procedure was also used for the catalytic growth of Ge nanowires, except for the powder and substrate temperatures, which are lowered to $\sim$ 600 °C and $\sim$ 450 °C, respectively.

For oxide-assisted growth, SiO powders were evaporated at 1400 °C in an alumina tube, while a 50-sccm Ar flow (400–800 mbar) was maintained for the length of the whole process. The SiO vapour is found to condense sharply in the form of nanowire bundles at 950 °C. A cylindrical quartz ring matching the main tube diameter was used to allow easy collection of the as-grown material without need for any disruptive mechanical action.

For thermolysis growth, we prepared patterned micropillar structures where a 10-nm-thick Au layer was evaporated on top of a 200-nm-thick $SiO_x$ terrace deposited by magnetron sputtering. The samples were then placed in a quartz boat and annealed for 2 h at 1200 °C, resulting in the growth of SiNWs. A constant $N_2$ flux (1 l/min) was supplied at atmospheric pressure for the whole duration of the synthesis run.

Raman spectroscopy and photoluminescence (PL) were measured at room temperature using a 514.5-nm Ar-ion laser excitation coupled with a Renishaw micro-Raman spectrometer.

## 3 Results and discussion

### 3.1 *SiNW synthesis*

We first discuss the growth of Si NWs by thermal CVD and PECVD using $SiH_4$ as the Si source gas and Au as the catalyst. The substrate temperature was kept to relatively low values (300–380 °C), as our aim in developing a NW growth recipe for (PE)CVD is to ensure wide compatibility in terms of available substrates and fabrication schemes. At $SiH_4$ pressures of 1 Torr and below, a negligible yield of Si NWs is observed without plasma. Under the same conditions of temperature and pressure, the use of a 10-W rf plasma resulted in the growth of micron-long SiNWs a few nanometres in diameter [7], Fig. 1a. The Si NWs in Fig. 1a originate from patterned Au islands and extend onto the Au-uncoated regions that did not react with the $SiH_4$ precursor. A high-resolution transmission electron microscopy (HRTEM) micrograph of a single SiNW is shown in Fig. 1b. The wire is fairly uniform in diameter and exhibits a highly crystalline Si core, about 7–8 nm in diameter, surrounded by a 1–2 nm amorphous shell. As shown in Fig. 2, elemental mapping by electron energy loss spectroscopy (EELS) [7] further confirms that the NW Si core is surrounded by $\sim$ 2 nm of $SiO_x$. The analysis was performed in a field-emission-gun TEM operated at 300 kV, the chemical maps representing the projected elemental concentrations in the electron-beam direction. The $SiO_x$ layer is most likely native Si oxide formed during extended air exposure after deposition.

Figure 3a shows SiNWs thermally grown at 3 Torr on a uniform Au catalyst layer. Such NWs are structurally equivalent to those produced by PECVD at 1 Torr and shown in Figs. 1 and 2. In Fig. 3b, we show SiNWs grown at 3 Torr but with the use of a 10-W plasma. In this case, the catalytic growth rate has been dramatically enhanced as the wires are now tenths of microns in length. However, they look

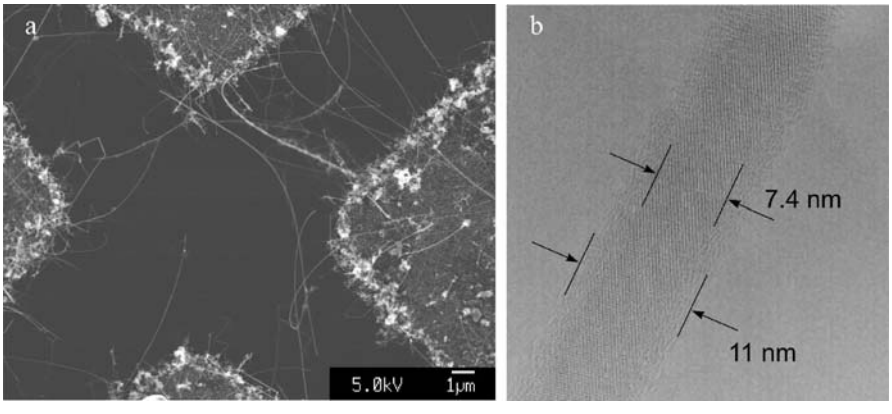


**FIGURE 1** (**a**) Scanning electron microscope image of PECVD-grown SiNWs nucleating on patterned Au catalyst islands. (**b**) HRTEM micrograph of a 10-nm-thick SiNW, showing the crystalline Si core surrounded by an amorphous shell

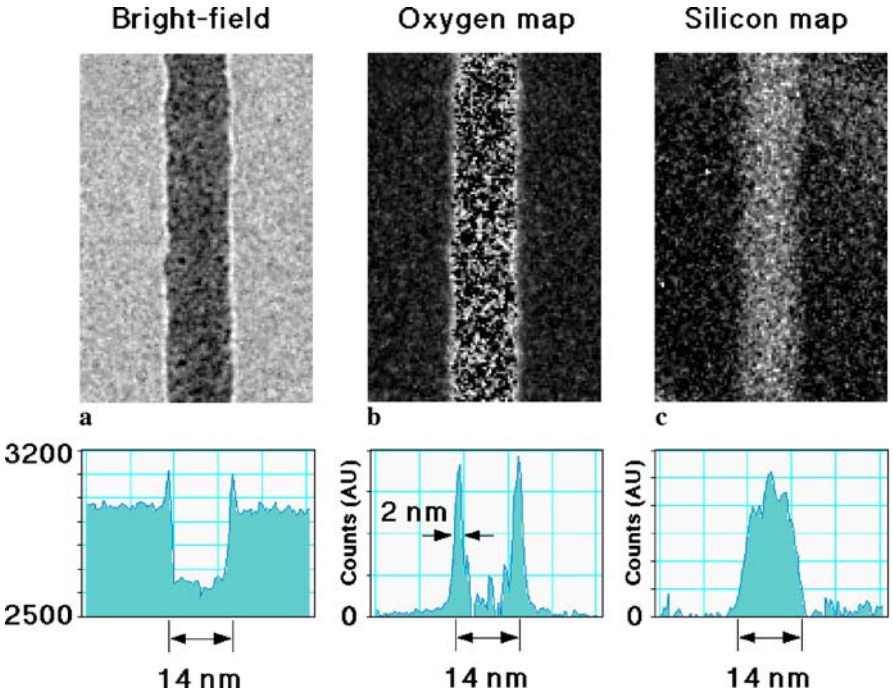


**FIGURE 2** EELS elemental maps of a 14-nm-diameter SiNW. The bright-field image was acquired slightly under focus (**a**). Three-window background-subtracted elemental maps were acquired using the oxygen *K* edge (532 eV) (**b**) and the Si *K* edge (1839 eV) (**c**) on a CCD camera. The 2-nm-thick $SiO_x$ sheath corresponds well with the outer amorphous layer seen in the HRTEM analysis in Fig. 1b

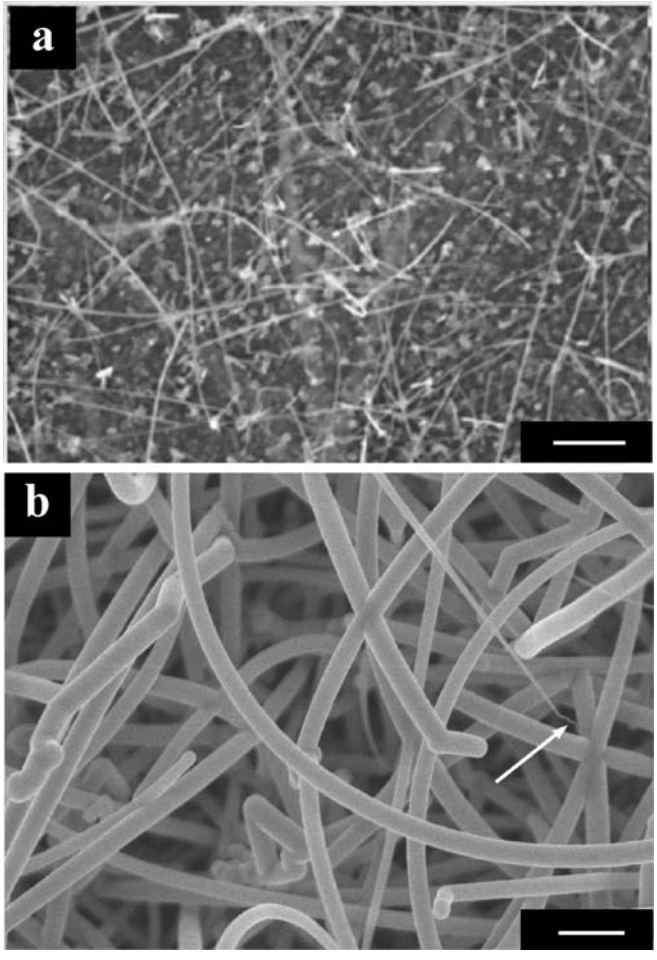


**FIGURE 3** (**a**) SiNWs grown at 3 Torr without plasma on a uniform Au catalyst layer. *Scale bar*: 500 nm. (**b**) SiNWs grown at 3 Torr but with the use of a 10-W plasma. Wires are tenths of microns in length and tapered, as deduced by their larger average diameter and by the presence of sharp tips where the Au catalyst particle can still be found (see *arrow*). *Scale bar*: 1 μm

much thicker (200–300 nm) and tapered, indicating that Si overgrowth on the NW side walls also occurred during the deposition process.

The uncatalysed Si deposition and catalysed SiNW growth always coexist in the CVD process. A key role of Au is to make the catalytic process dominant under given conditions. We emphasize that Au-catalysed NW growth does not fundamentally validate the proposed vapour–liquid–solid (VLS) nucleation model [20, 21]. Nominally sub-eutectic NW synthesis using Au as catalyst has been achieved for several semiconductor materials, including Ge [22], InP [23], and ZnSe [24]. Therefore, the synthesis of SiNWs at 300 °C (well below the minimum Au–Si eutectic temperature of 363 °C) is more consistent with a solid-phase catalytic reaction [23, 24].

Thus, for low-temperature CVD growth of SiNWs, a relatively high pressure of $SiH_4$ is needed to promote 1D nucleation. An applied rf plasma is beneficial for the catalyst-driven growth mechanism, since it allows the synthesis of SiNWs at lower pressures and higher growth rates. However, catalyst-free Si deposition is increased as well within this regime. By choosing the proper combination of parameters, the longitudinal and radial growth rates may be controlled to yield SiNWs with the desired shape and aspect ratio.

We now consider SiNWs grown by thermal evaporation. Bulk quantities of free-standing SiNWs are deposited by a solid–vapour process in a high-temperature furnace reactor (Fig. 4). Si or SiO powders were placed in an alumina boat and heated at 1200 °C and 1400 °C, respectively. Au-coated substrates were held in the low-temperature zone of the tube in the downstream direction of an inert-gas flow. Furnace SiNW growth can be either catalyst-assisted or catalyst-free. The catalyst-free mechanism is often referred to as oxide-assisted growth, to stress the critical role of oxygen in triggering the growth of SiNWs [25]. SiO powder has to be used in this case, as no self-assembled SiNWs are found on the tube walls by using pure Si as solid precursor. According to Zhang et

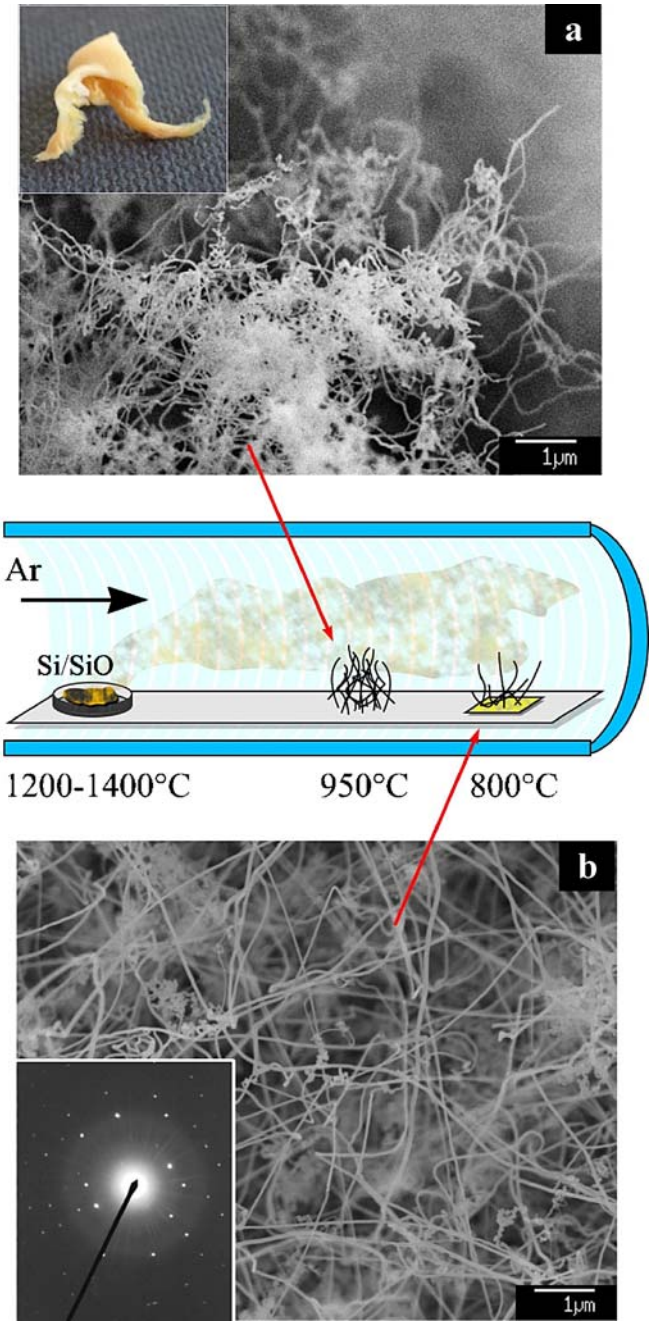


**FIGURE 4** Bulk production of SiNWs obtained in our horizontal-tube furnace by vapour transport of thermally evaporated Si or SiO powders. (**a**) By using SiO as precursor large bundles of SiNWs condense on the tube walls around 950 °C. The *inset* shows the as-grown raw material on a 1 : 1 scale. (**b**) Metal-catalysed growth is achieved by placing Au-coated substrates at temperatures around 800 °C

al. [25], $SiO_x$ clusters condense preferentially at the wire tip providing the desired one-dimensional growth, while a $SiO_2$ shell is formed on the sides avoiding further lateral sticking of vapour. The Au-catalysed mechanism, on the other hand, yields similar SiNWs irrespective if Si or SiO powders are used.

Figure 4a and b show SiNWs fabricated by the oxide-assisted and Au-catalysed synthesis methods, respectively. Several milligrams of SiNWs were produced in (a), the inset showing an as-grown pure-SiNW bundle on a 1 : 1 scale. A dense forest of SiNWs was produced in (b), yet the yield was limited in this case by imposing the nucleation to take place only on an Au-coated surface. Despite the very different mechanisms responsible for NW growth in (a) and (b), we found that both approaches led to a similar final morphology. Indeed, wire length and diameter are closely comparable, the former being up to tenths of microns, the latter as small as 10–30 nm. Interestingly, both types of wires show the same degree of curliness, in contrast to (PE)CVD wires shown in Figs. 1–3 that are usually very straight or sharply kinked. For (PE)CVD-grown SiNWs, a curly morphology was considered a fingerprint of amorphous structures [6, 7]. However, a selected-area diffraction pattern (SADP) taken by TEM on a single isolated NW from Fig. 4b (inset) indicates that these wires are crystalline Si, though most of the considered patterns were hardly found to be single crystals, but rather made of multiple crystalline domains.

The vapour-transport method is applicable to a large class of materials [19, 25–27]. For instance, Au-catalysed GeNWs grown in our system by thermal evaporation of Ge powders are shown in Fig. 6. A morphology trend is extracted for independently varying the powder temperature ($T_P$) and the substrate temperature ($T_S$). Long and thin NWs ($\sim 50$ nm in diameter) are obtained at $T_P = 650\,^\circ$C, $T_S = 450\,^\circ$C. Thicker wires up to 300 nm in diameter are found by increasing both temperatures to $T_P = 700\,^\circ$C and $T_S = 500\,^\circ$C. For fixed $T_P = 700\,^\circ$C, lowering $T_S$ to 425 °C gives rise to nanosaws with irregular teeth profiles. Such a trend is fully consistent with our previous reports on CdSe and ZnTe NWs grown by vapour transport [19, 28], indicating the general validity of the vapour-transport growth model outlined there. It is also notable that GeNWs grown by vapour transport are straight, in contrast with SiNWs that exhibit a high degree of curliness (Fig. 4). This demonstrates that our vapour-transport furnace is intrinsically suitable for the production of high-crystal-quality NWs. We speculate that SiNW curliness and fragmentation into crystalline domains might be due to the high nucleation temperatures (800–950 °C). An excess of thermal energy is likely to overrule the differences in surface energies that lead to a stable and well-defined growth direction for SiNWs of fixed diameter [29]. For high-density, large-diameter NWs (100–500 nm), branched structures are sometimes observed (see Figs. 3b and 5). We believe that the branching is not due to individual NWs splitting during growth, but rather due to the interference among close-packed multiple NWs (which increases with the NW average thickness). In high-density arrays, two NW tips may collide during growth and merge together, continuing the nucleation process as a single front. Alternatively, two thin NWs in close proximity may compenetrate each other as long as lateral overgrowth occurs.

Oxide-assisted growth of Ge NWs has also been demonstrated [30]. It becomes evident that the main advantage of the vapour-transport approach is versatility; using a relatively cheap experimental set-up, NWs of different materials are easily synthesized without the need for dangerous precursor gases such as $SiH_4$ or $GeH_4$. On the other hand, the high temperatures involved in the process do limit the substrate selection. Nanowires grown by this technique look more suitable

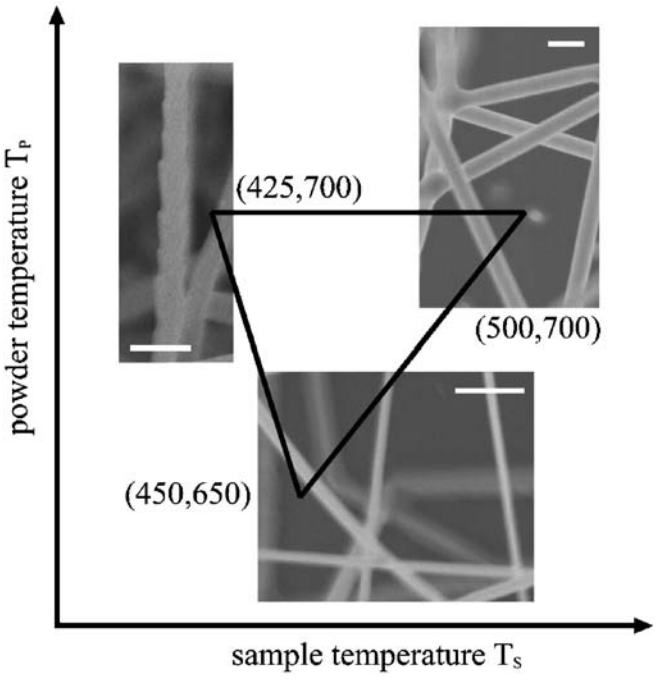


**FIGURE 5** Au-catalysed Ge NWs grown by vapour transport for different combinations of sample temperature and powder temperature ($T_S$, $T_P$). Thin NWs, thick NWs, and nanosaws can be obtained according to a well-establish deposition trend [19, 28]. All the synthesized GeNWs are straight over lengths of several microns. *Scale bars*: 500 nm

for assembly strategies that involve NW dispersion in solution for post-growth processing [31].

Selective growth can also be achieved in a furnace by annealing pre-patterned precursor films. This synthesis approach is simpler than gas-phase methods as it involves a smaller number of deposition parameters. We have synthesized core/shell $Si/SiO_2$ nanowires by annealing pre-patterned $SiO_2$/Au vertical heterostructures [32]. Figure 6a shows an array of NW bushes originating from precursor islands $\sim 2\,\mu$m in diameter. Every set of wires originates from a specific location independently of the neighbouring islands and with a thickness between 200 and 400 nm. No structures form outside the pre-patterned regions. The wires show a preferential vertical alignment, possibly occurring because of the vapour-diffusion direction from bottom to top (opposite to vapour diffusion from precursor powders in Fig. 4). By further scaling the pattern features to less than 1 μm, single nanowires per island can be obtained, in a similar fashion to that achieved for growth of single carbon nanofibres [33].

### 3.2 *Optical properties*

As for carbon nanotubes, Raman spectroscopy is a preferred tool for the non-destructive characterization of SiNWs and a direct probe for quantum confinement effects. The selection rule $q = 0$ for bulk crystals is relaxed in NWs of small diameter, as the participation of phonons near the Brillouin zone centre becomes allowed under the Heisenberg uncertainty principle. For Si, this activates lower-frequency optical phonons. Therefore, the first-order Raman Si peak ($520\,\mathrm{cm}^{-1}$) is predicted to show an asymmetric broadening and down shift [34, 35]. We calculate the down shift to be about $1\,\mathrm{cm}^{-1}$ for wires 10 nm in diameter [36]. Some papers found larger shifts ($15$–$20\,\mathrm{cm}^{-1}$) in the main Si peak, varying with laser power and wavelength, which are attributed to resonant selection of wires of different diameter or to electronic Raman scattering [37, 38]. We argue against this interpretation.

Several spectra were acquired at 514.5-nm excitation with a $\times 100$ objective and a laser power of 0.02–2.6 mW. The SiNW spectra are found to broaden and down shift significantly when increasing the laser power, Fig. 7a. This effect cannot be attributed to phonon confinement. Figure 7b shows that the anti-Stokes/Stokes intensity ratio increases with laser power for a SiNW, whereas it is constant for bulk Si, indicating a very high local temperature for high powers. Very low power must therefore be used in order to avoid local heating of SiNWs. The high sensitivity of SiNWs to laser irradiation shows that thermal conductivity of SiNWs is much lower than for bulk Si [36], as validated by direct thermal conductivity measurements [39].

In Fig. 8, we compare the first-order Raman peak down shift for SiNWs grown by different techniques. Au-catalysed SiNWs, prepared both by CVD and by vapour transport on quartz substrates, were measured directly on their substrates. As-grown SiNW bundles prepared by the oxide-assisted method were mechanically flattened and illuminated without further processing. For all wires, a similar trend is observed as a function of the laser power, consistently with previous experiments [36]. This implies that different synthesis methods, including the use of a metallic catalyst or different nucleation temperatures, do not sensibly affect the resulting thermal conductivity of nominally intrinsic SiNWs.

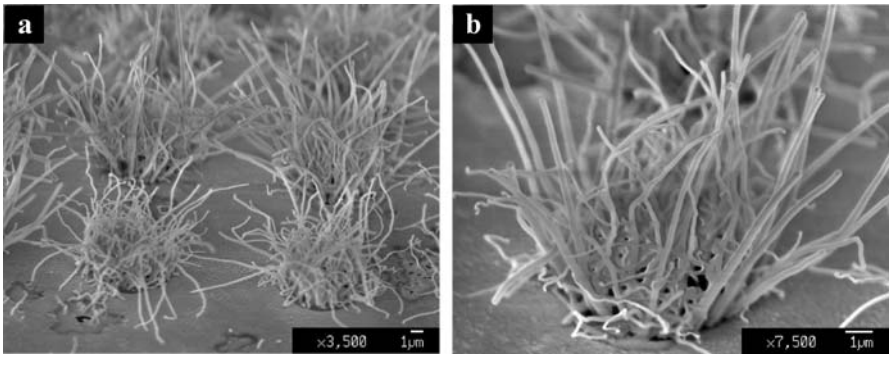


**FIGURE 6** (**a**) SiNW bushes nucleating from lithography patterned micropillars. (**b**) A close-up of an individual NW bush, showing the selectivity of the thermolysis process and the preferential vertical alignment of the resulting NWs

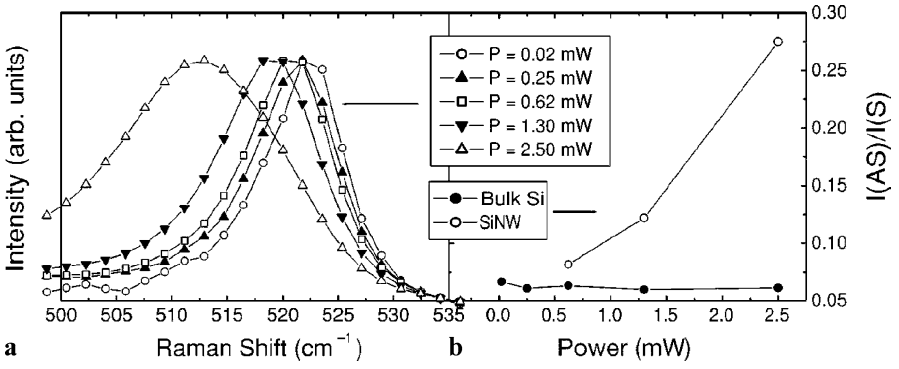


**FIGURE 7** (**a**) SiNW Raman spectra at 514.5 nm for increasing laser power. (**b**) $I(\mathrm{AS})/I(\mathrm{S})$ as a function of laser power for SiNW and bulk Si

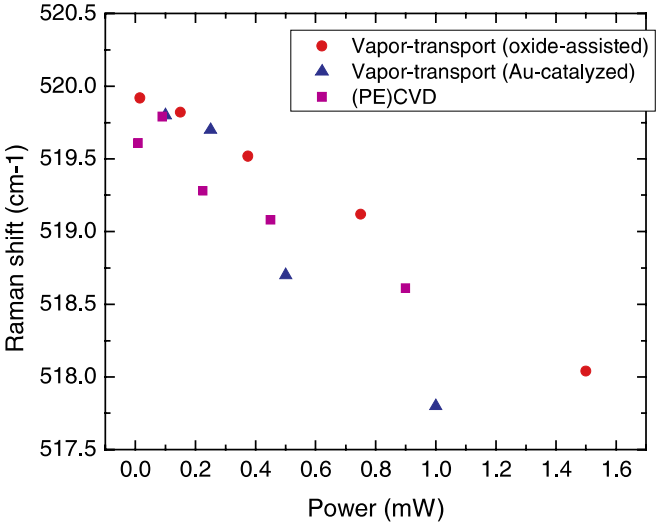


**FIGURE 8** Raman shift as a function of laser power for SiNWs grown by different techniques. A similar down shift of the first-order Si peak is measured in all cases. The Au-catalysed NWs grown by vapour transport appear to heat up most easily with increasing power

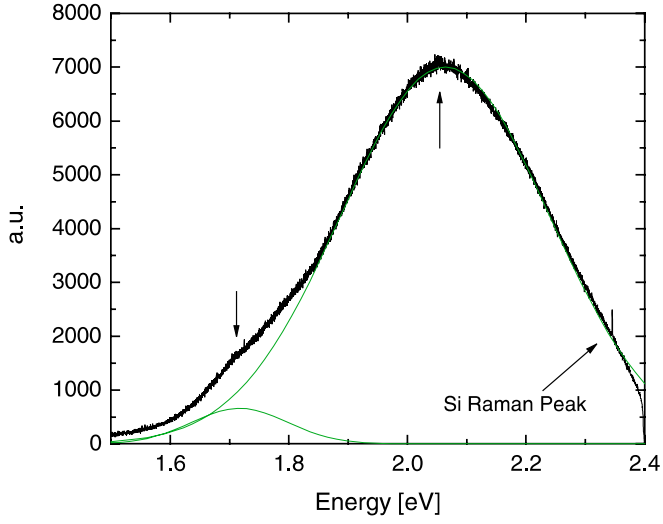


**FIGURE 9** Photoluminescence spectrum taken at room temperature for oxide-assisted-growth SiNWs bundles. A main green emission at 2.05 eV and a smaller red contribution at $\sim 1.7$ eV are seen

Since the proposal that efficient visible-light emission from high-porosity structures arises from quantum confinement effects, porous Si and Si nanocrystals have received increasing interest as potential novel materials for optoelectronic and photovoltaic applications [40, 41]. Unlike bulk Si, a SiNW can become a direct band gap semiconductor at nanometre diameter [40]. The origin of optically and electrically stimulated emission of nanosize Si, however, has been controversial. Multiple bands have been observed, spanning from near-infrared to ultraviolet wavelengths, and tentatively assigned to contaminated or defective Si oxide, dangling bonds, and quantum confinement effects [41, 42].

We performed PL studies of oxide-assisted-grown SiNWs. Au is known to be a deep-level acceptor and recombination centre in Si [43]. Thus, metal-free, self-catalysed SiNWs appear to be the best candidates for optoelectronic applications. In addition, we observed that these wires typically exhibit the smallest average diameter (crystalline core is $\sim 10$ nm or lower), and measured in bulk quantities they are likely to yield the strongest signal intensity.

Figure 9 shows a PL spectrum of as-grown SiNWs bundles synthesized by the oxide-assisted method. A major broad band is found around 2.05 eV. Such green–blue emission is often seen for SiNWs, and it may be attributed to recombination in the oxide shell [44, 45]. An additional peak or shoulder is visible at 1.7 eV. The red emission from nanocrystalline Si is related to quantum confinement effects [41, 42, 45]. Bai et al. [46] however noted that confinement-related emission should be negligible if the SiNW diameter is larger than the Bohr radius in Si ($\sim 5$ nm). They proposed that structural defects, such as stacking faults and twin boundaries, are responsible for the red fluorescence. Similar arguments might be applied to our SiNWs as well, because our wire diameters are on the same scale ($\sim 10$ nm). Further insights may be extracted by oxidizing the as-grown SiNWs to reduce the nanocrystal size or by chemical treatments of the oxide shells [41, 46]. As a relatively high laser power is needed to assess the PL of SiNWs, due to their low emission efficiency, the heating effects outlined in discussing the Raman data should also be taken into account.

## 4 Conclusion

We have investigated and compared multiple routes to SiNW synthesis. As a function of the selected deposition technique, we achieved different yields, selective Au-catalysed growth, bulk catalyst-free production, and relatively high or low nucleation temperatures. The final morphology of NWs is also strongly process dependent. In terms of optical properties, however, similar behaviours are observed. The

large down shift of the Si Raman peak for increasing laser power is attributed to heating effects due to the poor thermal conductivity of all SiNWs explored.

**ACKNOWLEDGEMENTS** This work was supported in part by the EU project CANAPE. We acknowledge funding from Peterhouse College, Pembroke College, EPSRC, The Royal Society, The Leverhulme Trust.

## REFERENCES

1 X. Duan, Y. Huang, R. Agarwal, C.M. Lieber, Nature **421**, 241 (2003)
2 M.H. Huang, S. Mao, H. Feick, H. Yan, Y. Wu, H. Kind, E. Weber, R. Russo, P. Yang, Science **292**, 1897 (2001)
3 X. Duan, C. Niu, V. Sahi, J. Chen, J.W. Parce, S. Empedocles, J.L. Goldman, Nature **425**, 274 (2003)
4 V. Schmidt, H. Riel, S. Senz, S. Karg, W. Riess, U. Gosele, Small **2**, 85 (2006)
5 Y. Cui, Z. Zhong, D. Wang, W.U. Wang, C.M. Lieber, Nano Lett. **3**, 149 (2003)
6 J. Westwater, D.P. Gosain, S. Tomiya, S. Usui, H. Ruda, J. Vac. Sci. Technol. B **15**, 554 (1997)
7 S. Hofmann, C. Ducati, R.J. Neill, S. Piscanec, A.C. Ferrari, J. Geng, R.E. Dunin-Borkowski, J. Robertson, J. Appl. Phys. **94**, 6005 (2003)
8 Y. Cui, L.J. Lauhon, M.S. Gudiksen, J. Wang, C.M. Lieber, Appl. Phys. Lett. **78**, 2214 (2001)
9 A.I. Hochbaum, R. Fan, R. He, P. Yang, Nano Lett. **5**, 457 (2005)
10 G. Zheng, W. Lu, S. Jin, C.M. Lieber, Adv. Mater. **16**, 1890 (2004)
11 Y. Cui, X. Duan, J. Hu, C.M. Lieber, J. Phys. Chem. B **104**, 5213 (2000)
12 A.M. Morales, C.M. Lieber, Science **279**, 208 (1998)
13 Y.F. Zhang, Y.H. Tang, N. Wang, D.P. Yu, C.S. Lee, I. Bello, S.T. Lee, Appl. Phys. Lett. **72**, 1835 (1998)
14 D.P. Yu, Z.G. Bai, Y. Ding, Q.L. Hang, H.Z. Zhang, J.J. Wang, Y.H. Zou, W. Qian, G.C. Xiong, H.T. Zhou, S.Q. Feng, Appl. Phys. Lett. **72**, 3458 (1998)
15 F.M. Kolb, H. Hofmeister, R. Scholz, M. Zacharias, U. Gosele, D.D. Ma, S.T. Lee, J. Electrochem. Soc. **151**, G472 (2004)
16 J. Hu, Y. Bando, J. Zhan, Z. Liu, D. Golberg, S.P. Ringer, Adv. Mater. **17**, 975 (2005)
17 Y.F. Zhang, Y.H. Tang, C. Lam, N. Wang, C.S. Lee, I. Bello, S.T. Lee, J. Cryst. Growth **212**, 115 (2000)
18 Z.W. Pan, Z.R. Dai, L. Xu, S.T. Lee, Z.L. Wang, J. Phys. Chem. B **105**, 2507 (2001)
19 A. Colli, A. Fasoli, S. Hofmann, C. Ducati, J. Robertson, A.C. Ferrari, Nanotechnology **17**, 1046 (2006)
20 R.S. Wagner, W.C. Ellis, Appl. Phys. Lett. **4**, 89 (1964)
21 E.I. Givargizov, J. Cryst. Growth **31**, 20 (1975)
22 A.B. Greytak, L.J. Lauhon, M.S. Gudiksen, C.M. Lieber, Appl. Phys. Lett. **84**, 4176 (2004)
23 K.A. Dick, K. Deppert, T. Martensson, B. Mandl, L. Samuelson, W. Seifert, Nano Lett. **5**, 761 (2005)
24 A. Colli, S. Hofmann, A.C. Ferrari, C. Ducati, F. Martelli, S. Rubini, S. Cabrini, A. Franciosi, J. Robertson, Appl. Phys. Lett. **86**, 153 103 (2005)
25 R.Q. Zhang, Y. Lifshitz, S.T. Lee, Adv. Mater. **15**, 635 (2003)
26 G. Gu, M. Burghard, G.T. Kim, G.S. Dusberg, P.W. Chiu, V. Krstic, S. Roth, W.Q. Han, J. Appl. Phys. **90**, 5747 (2001)
27 Z.R. Dai, Z.W. Pan, Z.L. Wang, Adv. Funct. Mater. **13**, 9 (2003)
28 A. Fasoli, A. Colli, S. Hofmann, C. Ducati, J. Robertson, A.C. Ferrari, Phys. Status Solidi, unpublished
29 Y. Wu, Y. Cui, L. Huynh, C.J. Barrelet, D.C. Bell, C.M. Lieber, Nano Lett. **4**, 433 (2004)
30 Y.F. Zhang, Y.H. Tang, N. Wang, C.S. Lee, I. Bello, S.T. Lee, Phys. Rev. B **61**, 4518 (2000)
31 D. Whang, S. Jin, Y. Wu, C.M. Lieber, Nano Lett. **3**, 1255 (2003)
32 A. Colli, A.C. Ferrari, S. Hofmann, J.A. Zapien, Y. Lifshitz, S.T. Lee, S. Piscanec, M. Cantoro, J. Robertson, AIP Conf. Proc. **723**, 445 (2004)
33 S. Hofmann, C. Ducati, B. Kleinsorge, J. Robertson, Appl. Phys. Lett. **83**, 135 (2003)
34 I.H. Campbell, P.M. Fauchet, Solid State Commun. **58**, 739 (1986)
35 H. Richter, Z.P. Wang, L. Ley, Solid State Commun. **39**, 625 (1981)
36 S. Piscanec, M. Cantoro, A.C. Ferrari, A. Zapien, Y. Lifshitz, S.T. Lee, S. Hofmann, J. Robertson, Phys. Rev. B **68**, 241 312(R) (2003)
37 S.-L. Zhang, W. Ding, Y. Yan, J. Qu, B. Li, L. Li, K.T. Yue, D. Yu, Appl. Phys. Lett. **81**, 4446 (2002)
38 R. Gupta, Q. Xiong, C.K. Adu, U.J. Kim, P.C. Eklund, Nano Lett. **3**, 627 (2003)
39 D. Li, Y. Wu, P. Kim, L. Shi, P. Yang, A. Majumdar, Appl. Phys. Lett. **83**, 2934 (2003)
40 L.T. Canham, Appl. Phys. Lett. **57**, 1046 (1990); V. Lehmann, U. Gosele, Appl. Phys. Lett. **58**, 856 (1991)
41 F. Koch, V. Petrova-Koch, T. Muschik, J. Luminesc. **57**, 271 (1993)
42 P.M. Fauchet, J. Luminesc. **70**, 294 (1996)
43 D.V. Lang, H.G. Grimmeiss, E. Meijer, M. Jaros, Phys. Rev. B **22**, 3917 (1980)
44 X.H. Sun, N.B. Wong, C.P. Li, S.T. Lee, T.K. Sham, Appl. Phys. Lett. **96**, 3447 (2004)
45 M.V. Wolkin, J. Jorne, P.M. Fauchet, G. Allan, C. Delarue, Phys. Rev. Lett. **82**, 197 (1999)
46 Z.G. Bai, D.P. Yu, J.J. Wang, Y.H. Zou, W. Qian, J.S. Fu, S.Q. Feng, J. Xu, L.P. You, Mater. Sci. Eng. B **72**, 117 (2000)